



Understanding of atmospheric aerosol particles with improved particle identification and quantification by single particle mass spectrometry

Xiaoli Shen^{1,2}, Harald Saathoff^{1,*}, Wei Huang^{1,2}, Claudia Mohr^{1,3}, Ramakrishna Ramisetty^{1,4}, Thomas
5 Leisner^{1,5}

¹Institute of Meteorology and Climate Research, Karlsruhe Institute of Technology, Hermann-von-Helmholtz-Platz 1, 76344 Eggenstein-Leopoldshafen, Germany

²Institute of Geography and Geoecology, Working Group for Environmental Mineralogy and Environmental System Analysis, Karlsruhe Institute of Technology, Kaiserstr.12, 76131 Karlsruhe, Germany

10 ³Department of Environmental Science and Analytical Chemistry, Stockholm University, Stockholm, 11418, Sweden

⁴Now at: TSI Instruments India Private Limited, Bangalore, 560102, India

⁵Institute of Environmental Physics, University Heidelberg, In Neuenheimer Feld 229, 69120 Heidelberg, Germany

*Correspondence to: Harald Saathoff (harald.saathoff@kit.edu)

Abstract. Single particle mass spectrometry (SPMS) is a useful, albeit not fully quantitative tool to determine chemical
15 composition and mixing state of aerosol particles in the atmosphere. During a six-week field campaign in summer 2016 at a rural site in the upper Rhine valley near Karlsruhe city in southwest Germany, $\sim 3.7 \times 10^5$ single particles were analysed by a laser ablation aerosol particle time-of-flight mass spectrometer (LAAPTOF). Combining fuzzy classification, marker peaks, typical peak ratios, and laboratory-based reference spectra, seven major particle classes were identified. With the precise
20 identification and well characterized overall detection efficiency (ODE) for this instrument, particle similarity can be transferred into corrected number fractions and further transferred into mass fractions. Considering the entire measurement period, “Potassium rich and aromatics coated dust” (class 5) dominated the particle number (46.5% number fraction) and mass (36.0% mass fraction); “Sodium salts like particles” (class 3) were the second lowest in number (3.5%), but the second
25 dominating class in terms of particle mass (25.3%). This difference demonstrates the crucial role of particle mass quantification for SPMS data. Using corrections for maximum, mean, and minimum ODE, the total mass of the quantified particles measured by LAAPTOF accounts for $\sim 12\%$, $\sim 25\%$, and $\sim 104\%$ of the total mass measured by an aerosol mass spectrometer (AMS) with a collection efficiency of 0.5. These two mass spectrometers show a good correlation (correlation coefficient $\gamma > 0.6$) regarding total mass for more than 70% of the measurement time, indicating non-refractory species measured by AMS might originate from particles consisting of internally mixed non-refractory and refractory components. In addition, specific relationships of LAAPTOF ion intensities and AMS mass concentrations for non-refractory compounds
30 were found for specific measurement periods. Furthermore, our approach allows for the first time to assign the non-refractory compounds measured by AMS to different particle classes. Overall AMS-nitrate was mainly arising from class 3, while class 5 was dominant during events rich in organic aerosol particles.

1 Introduction

Life times of ambient aerosol particles range from hours to a few weeks, except for newly formed particles (~ 3 to 5 nm),
35 which have a predicted short lifetime of seconds (Pöschl, 2005). The atmospheric evolution of aerosol particles can alter their internal and external mixing states, as well as their chemical and physical properties, e.g., they can acquire coatings of secondary inorganic (sulfates, nitrates, and ammonium) and secondary organic compounds (Fuzzi et al., 2015). Hence, most aerosol particles are relatively complex mixtures, difficult to distinguish and to trace to their primary source and/ or secondary formation pathway. Single particle mass spectrometry (SPMS) has the capability of measuring most components



of the particles in real time, thus it has been a widely used technique to investigate mixing state and aging of aerosol particles for many years (Murphy, 2007; Noble and Prather, 2000; Pratt and Prather, 2012). However, SPMS data analysis has been proven difficult under real world conditions.

Particle type identification, i.e., the assignment of every detected particle to one out of a set of particle types, which are either predefined or deduced from the experimental data, is perhaps one of the most critical issues. Due to the relatively complex ablation and ionization mechanisms, including charge and proton transfer, as well as ion-molecule reactions that may occur in the plume with many collisions (Murphy, 2007; Reinard and Johnston, 2008), mass spectroscopic signatures do not necessarily reflect the primary composition of the particles. Several particle type identification methods were reported in previous studies: Gallavardin et al. (2008) used a pair of peak area ratios, such as $\text{Ca}_2\text{O}^+/\text{Ca}^+$ vs CaO^+/Ca^+ and $\text{SiO}^+/\text{SiO}_2^-$ vs $\text{SiO}_3^-/\text{SiO}_2^-$, to differentiate calcium/silicon containing mineral dust. Normalized histograms of $\text{PO}_3^-/\text{PO}_2^-$ and CN^-/CNO^- ratios were used to identify primary biological aerosol particles (Zawadowicz et al., 2017). Setting thresholds for marker peak signals can also help to classify and further identify specific particles (Köllner et al., 2017). Lu et al. (2018) used natural silicon isotopic signatures to study the sources of airborne fine particulate matter ($\text{PM}_{2.5}$), which shows how useful isotopic signatures can be for particle identification. A combination of peak area and peak shift ratio, based on subtle changes in ion arrival times in the mass spectrometer, was introduced by Marsden et al. (2018a) for the differentiation of mineral phases in silicates. Ternary sub-composition systems, such as $(\text{Al}+\text{Si})^+-\text{K}^+-\text{Na}^+$ and $\text{Cl}^--(\text{CN}+\text{CNO})^--\text{SO}_4^-$, were used to identify mineralogy and internal mixing state of ambient particles (Marsden et al., 2018b). In our previous study (Shen et al., 2018), laboratory-based reference spectra were suggested to be a useful tool for particle identification. These methods guide the way for improving the techniques to identify particle type and further identify individual aerosol particles.

An even more challenging issue is the quantitative analysis of individual particles' mass and chemical composition, which cannot be directly provided by SPMS measurements, because laser ablation only allows an a priori unknown fraction of the single particle to be vaporized and ionized (Murphy, 2007). In addition, matrix effects may obscure the particle composition (Gemayel et al., 2017; Gross et al., 2000). Our previous laboratory SPMS study also verified the difficulty of particle quantification due to incomplete ionization, which could not be improved significantly by replacing the originally used nanosecond excimer laser with a femtosecond laser with higher laser power density and shorter laser pulse length (Ramisetty et al., 2018). In the last two decades, great effort has been put into solving such quantification issues by using specific scaling or normalization methods. Gross et al. (2000) reported relative sensitivity factors (RSF) for ammonium and alkali metal cations in a SPMS to their corresponding bulk concentrations and accurately determined the relative amounts of Na^+ and K^+ in sea-salt particles. By normalizing the ion peak intensity of m/z 97⁺, 62⁺, 18⁺, 43⁺, and 36⁺ for sulfate, nitrate, ammonium, organic carbon (OC), and elemental carbon (EC), respectively, to number and size distribution data, Jeong et al. (2011) were able to detect a strong correlation between SPMS results and bulk measurements done for non-refractory material by an aerosol mass spectrometer (AMS). This scaling approach was improved by applying a hit rate correction (Zhou et al., 2016). Combining AMS, optical particle counter (OPC), and SPMS data, Gemayel et al. (2017) also quantified the fragments aforementioned in size-segregated atmospheric aerosols measured by SPMS in the field. In addition, Ahern et al. (2016) used the peak area ratio of organic matter marker at m/z 28 CO^+ to EC markers (C_{2-5}^+) to account for laser shot-to-shot variability, and demonstrated a linear relationship between normalized organic intensity and secondary organic aerosol (SOA) coating thickness on soot particles. To the best of our knowledge, all the previous SPMS quantification methods focused on some components of the aerosol particles, and most of them are based on comparison with reference instruments.

In this study, ambient aerosol particles were analysed in summer 2016 at a rural site in the upper Rhine valley of Germany using a laser ablation aerosol particle time-of-flight mass spectrometer (LAAPTOF, AeroMegt GmbH). Seven major particle classes were found among a total of $\sim 3.7 \times 10^5$ measured single particles. We developed a semi-quantitative method to estimate mass contributions for individual aerosol particles. In addition, we have found specific relationships of LAAPTOF ion intensity and AMS mass concentration results for non-refractory compounds, which might help estimate the



mass of these compounds in future SPMS studies. Furthermore, we observed that all particles were complex mixtures of organic and inorganic compounds, and their external mixing state varied for different measurement periods. This provides different sources for the non-refractory species measured by AMS and indicates different sources of aerosol particles.

2 Methods

5 2.1 Measurement location and instrumentation

The measurements were made at a ground-based rural site from July 15th to September 1st, 2016 next to the tram line north of the village of Leopoldshafen, Germany (49°6'10.54" N, 8°24'26.07" E). This location is about 12 km north of Karlsruhe city with 300 thousand inhabitants and significant industry including a power plant and refineries (Hagemann et al., 2014). Besides, it is located in the upper Rhine valley. Ambient particles were sampled for mass spectroscopic analysis with a flow rate of 1 m³ h⁻¹ through a PM_{2.5} inlet (SH 2.5 - 16, Comde-Derenda GmbH) and vertical stainless steel tubes. A total suspended particulates (TSP) inlet (Comde-Derenda GmbH) was used for instruments for particle physical characterisation. Trace gases were sampled via an 8 mm PFA sampling tube. All sampling inlets were positioned 1.5 m above a measurement container and 3.7 m above ground level. To study the nature and to identify possible sources of the particles in this area, their number, size, chemical composition, and associated trace gases, as well as meteorological conditions were measured using the following instruments: Condensation particle counters (CPC3022A, CPC3772, TSI Inc.), optical particle counter (FIDAS, PALAS GmbH), aethalometer (AE33-7, Magee Scientific), ozone monitor (O341M, Environment SA), SO₂ monitor (AF22M Environment SA), NO₂ monitor (AS32M, Environment SA), CO₂ monitor (NGA2000, Rosemont Inc.), and meteorology sensors (WS700 & WS300, Lufft GmbH). From July 26th to August 31st, we deployed the mass spectrometers, e.g., a high resolution time-of-flight aerosol mass spectrometer (HR-ToF-AMS, Aerodyne Inc.), and a laser ablation aerosol particle time-of-flight mass spectrometer (LAAPTOF, AeroMegt GmbH), providing real time information on size and mass spectral patterns for bulk samples and individual particles, respectively.

The HR-ToF-AMS was designed to yield quantitative information (mass concentration) on size resolved particle bulk chemical composition with high time resolution and high sensitivity (DeCarlo et al., 2006). Briefly, aerosols are sampled with a flowrate of ~84 cm³ min⁻¹ via an aerodynamic lens, which focuses particles with sizes of 80 to 2500 nm (vacuum aerodynamic diameter, d_{va}) into a narrow beam. The particle beam passes through a sizing chamber where the particles' size is determined. Afterwards, particles encounter a 600 °C heater that vaporises the non-refractory species. The vapour is ionized by electron impact (electron energy: 70 eV). The generated positive ions are analysed by time-of-flight mass spectrometer. Particles can bounce off the heater/vaporizer, leading to an underestimation of ambient mass concentrations measured by AMS and thus a collection efficiency (CE, the product of net particle transmission and detection efficiency) < 1 (Canagaratna et al., 2007). It is important to note that the CE can vary depending on composition and phase of the particles (Bahreini et al., 2005). In this study, we applied a CE value 0.5, in accordance with previous studies (Canagaratna et al., 2007; Middlebrook et al., 2012) and in a related paper by Huang et al. (2018), the composition dependent CE has been calculated to have a very close value to 0.5.

The LAAPTOF is a commercially available SPMS and has been described elsewhere (Ahern et al., 2016; Gemayel et al., 2016; Marsden et al., 2016; Ramisetty et al., 2018; Reitz et al., 2016; Shen et al., 2018; Wonaschuetz et al., 2017). In brief, aerosols are sampled with a flowrate of ~80 cm³ min⁻¹ via an aerodynamic lens. Particles in a size range between 70 nm and 2500 nm d_{va} are focused and then accelerated. Afterwards, they pass through the detection chamber with two diode laser beams ($\lambda = 405$ nm). Once the single particle is coincidentally detected by both of the detection lasers, its aerodynamic size is determined and recorded, and an excimer laser ($\lambda = 193$ nm) is fired for a one step desorption/ionization of the refractory and non-refractory species of the particle. The resulting cations and anions are analysed by a bipolar time-of-flight mass spectrometer with unit mass resolution. Thus, for each individual particle a bipolar spectrum is generated.



2.2 Single particle identification and quantification methods for LAAPTOF data

The general data analysis procedures for particle spectral and size information was described in full detail in our previous study (Shen et al., 2018). Here, we extend this approach and apply it to a large atmospheric sample. We used the fuzzy *c*-means clustering algorithm embedded in the LAAPTOF Data Analysis Igor software (Version 1.0.2, AeroMegt GmbH) to find the major particle classes and their corresponding representative spectra, which were further correlated with laboratory-based reference spectra. The resulting correlation together with marker peaks (characteristic peaks arising from the corresponding species) and some typical peak ratios (e.g., isotopic ratio of potassium) was used to identify particle classes.

The fuzzy *c*-means clustering approach has the advantage of allowing particles to belong to multiple classes based on the similarity of the mass spectra (Reitz et al., 2016), namely, fractions of individual particles are assigned to different classes. A direct class-dependent quantification of particle mass is therefore not possible. In order to quantify particle mass, we first need to assign a particle class to every individual particle, which is achieved by correlating the individual bipolar mass spectra with the representative fuzzy class spectra using Pearson's correlation coefficient (γ). Since the positive LAAPTOF spectra are more characteristic than the negative ones (Shen et al., 2018), the threshold value for the positive spectra correlation was set to $\gamma_{\text{pos}} \geq 0.6$, while for the negative spectra γ_{neg} was tuned with different values varying from 0.3 to 0.8 (cf. Table S1). Individual particles whose γ for both spectra exceeds γ_{pos} and γ_{neg} when correlated to spectra of a certain class are assigned to this class. All corresponding correlation coefficients (γ_{pos} and γ_{neg}) are listed in Table S1. This way, we can obtain time series of particle counts, which has good ($\gamma > 0.6$)/strong correlation ($\gamma > 0.8$) with fuzzy results, and the corresponding correlation coefficients are also listed in Table S1, and typical examples are shown in Fig. S1. With this method, we were able to successfully classify 96% of the measured particles. Once the class information for individual particles has been determined, we are able to calculate single particle geometric size, volume and mass.

For simplicity, we assume the particles are spherical with a shape factor (χ) of 1, thus particle geometric diameter (d_p), volume (V_p) and mass (m_p) can be obtained from the following equations:

$$d_p = d_m = \frac{d_{va}}{\rho_p} \times \rho_0 \times \chi \quad (\chi = 1) \quad (\text{DeCarlo et al., 2004}) \quad (1)$$

$$V_p = \frac{1}{6} \times \pi \times d_p^3 \quad (2)$$

$$m_p = V_p \times \rho_p \quad (3)$$

where d_m is the electrical mobility diameter, d_{va} is the vacuum aerodynamic diameter measured by LAAPTOF, ρ_0 is the standard density (1 g cm^{-3}), and ρ_p is the particle density. Based on Eq. (1) to (3), we can deduce that m_p is proportional to $\chi^3 \rho_p^{-2}$. Please note that the shape factor χ of non-spherical particles is not equal to 1, e.g., $\chi_{\text{NaCl}} = 1.02\text{--}1.26$ (Wang et al., 2010) and $\chi_{\text{NH}_4\text{NO}_3} = 0.8$ (Williams et al., 2013). This causes an uncertainty of 26% for the particle diameter and 100% for the particle mass. Such an uncertainty is difficult to reduce, since we don't have particle shape information for individual particles. It should be noted that in previous studies, the particle shapes were also assumed as spherical, and averaged particle densities (~ 1.6 to 1.9 g cm^{-3}) based on the comparison between d_{va} and d_m were applied for total aerosol particle mass quantification (Gemayel et al., 2017; Jeong et al., 2011; Zhou et al., 2016). The density for different types of ambient particles varies, which will be shown in the following text. In order to reduce the uncertainty induced by the assumption of a uniform density, we assigned one density to each particle class and this density was used for the individual particles of each class. As discussed in the following Sect. 3.1, 7 major particle classes have been identified. Class 1, 5, and 6 are dust like particles and class 7 contains more mixed particles which also show good correlation to dust reference particles, thus we assumed the same density for class 1, 5, 6, and 7 as for dust, which is about 2.6 g cm^{-3} (Bergametti and Forêt, 2014). Class 2 particles are like aged soot for which we use a density of 1.8 g cm^{-3} as recommended by (Bond et al., 2013). Class 3 is sodium salts like particles, with relatively more sodium nitrate related markers, thus we assumed the density of sodium



nitrate (2.3 g cm^{-3}). Class 4 consists of relative fresh particles with strongest correlation to the mixture of ammonium sulfate (1.77 g cm^{-3}) and nitrate (1.73 g cm^{-3}), thus we assume the density as 1.75 g cm^{-3} .

Furthermore, the single particle identification allows for correcting the particle number counts by using the overall detection efficiency (ODE), which depends on particle size and type (Shen et al., 2018). Given the fact that ambient aerosol particles are complex mixtures, it is difficult to obtain a specific ODE for each particle class. If we used the estimated class dependent ODE, more uncertainties would be introduced and thus quantification complicated further. For simplicity and in order to account for different types of ambient particles, we averaged the ODE determined for ammonium nitrate, sodium chloride, PSL particles, and some other particles, e.g., agricultural soil dust, sea salt, organic acids, as well as secondary organic aerosol particles measured in the lab. The mean ODE with uncertainties as a function of particle size is shown in Fig. 1. The equations for correction and calculation of mass concentration are as follows:

$$\text{counts}_{\text{corrected}} = 1/\text{ODE}_{d_m} \quad (4)$$

$$\text{mass}_{\text{corrected}} = \text{counts}_{\text{corrected}} \times m_p \quad (5)$$

$$\text{mass concentration} = \text{Total mass}/(\text{sample flowrate} \times \text{time}) \quad (6)$$

where ODE_{d_m} is the mean ODE that depends on d_m ; $\text{counts}_{\text{corrected}}$ and $\text{mass}_{\text{corrected}}$ are the corrected particle number counts and mass at each time point; the sample flowrate is $\sim 80 \text{ cm}^3 \text{ min}^{-1}$. Furthermore, we can calculate the corrected number fractions and mass fractions once we have done the calculation according to Eq. (4) to (6).

The aforementioned assumptions and the related uncertainties in particle mass are summarised as follows: 1) ambient particles are spherical. This leads to an uncertainty of $\sim 100\%$ in particle mass; 2) particles in the same class have the same density. This leads to an uncertainty of $\sim 4\%$ in particle mass for ammonium salt particles with assumed density (ρ_{as}) of 1.75 g cm^{-3} , which is the averaged value from ammonium sulfate and nitrate with densities of 1.77 g cm^{-3} and 1.73 g cm^{-3} , respectively (Weast, 1987), $\sim 25\%$ for sodium salts particles with $\rho_{\text{as}} = 2.36 \text{ g cm}^{-3}$, averaged value from sodium nitrate, chloride, and sulfate with densities of 2.26, 2.17, and 2.67 g cm^{-3} , respectively (Weast, 1987), and much bigger uncertainty for soot particles with $\rho_{\text{as}} = 1.8 \text{ g cm}^{-3}$, due to their densities raging from < 1 to ~ 2 as a results of their aggregate structures (Bond et al., 2013); 3) the ODE is the same for all particles of the same size. This leads to an uncertainty of 500% in particle mass due to the variability of ODE values (Fig. 1). Obviously, this will lead to some bias. For example, if we apply ODE mean values to all the ambient particles, the number of ammonium nitrate rich particles might be overestimated due to the higher ODE of ammonium nitrate, while the ammonium sulfate rich, sea salt particles, and some organic rich such as organic acids rich particles might be underestimated.

Hence, the overall uncertainty in particle mass according to the assumptions is $\sim 540\%$ with the ODE caused uncertainty being dominant. This is because: 1) ambient particles are more complex than particles generated in the laboratory, e.g., concerning morphology or optical properties. These factors have a strong impact on ODE (Shen et al., 2018); 2) in this study most of the major particle classes in the ambient are dust like particles (cf. Sect. 3.1), but we only have the laboratory derived ODE for agricultural soil dust at around 300 nm; 3) instrumental aspects such as alignment and variance in particle-laser interaction lead to uncertainty in ODE. Considering the big uncertainty, our quantification method should be named semi-quantification.

3 Results and Discussion

3.1 Identification of particle classes and the internal mixing

During the six-week measurement campaign, $\sim 3.7 \times 10^5$ single particles bipolar LAAPTOF spectra were generated. From these data, seven major particle classes were found using fuzzy classification (Table 1). The corresponding representative spectra with marker peaks assignment and the size resolved number fraction of particle classes are shown in Fig. 2. Signatures for organic and secondary inorganic compounds can be observed in each class, i.e., for organics 24 C_2^- , $25 \text{ C}_2\text{H}^-$,



26 C_2H_2/CN^- , and 42 C_2H_2O/CNO^- , for sulfate 32 S^- , 64 SO_2^- , 80 SO_3^- , 81 HSO_3^- , 97 HSO_4^- , 177 $SO_3HSO_4^-$ and 195 $HSO_4H_2SO_4^-$, for nitrate 30 NO^+ , 46 NO_2^- , and 62 NO_3^- , and for ammonium 18 NH_4^+ and 30 NO^+ . Note that 30 NO^+ can not only originate from nitrate (majority), but also from ammonium (Murphy et al., 2006; Shen et al., 2018). Although different particle classes have similar fragments, they show characteristic patterns with several intensive marker peaks in the

5 corresponding spectra, which can be identified with the help of reference spectra (Shen et al., 2018).

After fuzzy classification each particle was tested for its similarity to the different particle classes. Although a similarity is not equal to the number fraction, they are related. A higher similarity of the total aerosol particles to one class indicates that a bigger number fraction of this class could be expected once the individual particles are assigned to it. As shown in Fig. 3a, the highest similarity (43.5% of all particles) is found to class 3, which is named “Sodium salts like particles” due to its

10 strong correlation ($\gamma \geq 0.8$) with Na salts (cf. Fig. 4). The spectra of this class in our study feature marker peaks arising from $NaNO_3$ (m/z 115 $Na(NO_2)_2^-$, 131 $NaNO_2NO_3^-$, and 147 $Na(NO_3)_2^-$), Na_2SO_4 (m/z 165 $Na_3SO_4^+$), and $NaCl$ (m/z 81/83 Na_2Cl^+ , 139/141 $Na_3Cl_2^+$, 35/37 Cl^- , and 93/95 $NaCl_2^-$). This class accounts for the largest fraction in the size range from 1000 to 2500 nm d_{va} (cf. Fig. 2). The size distribution of class 3 particles was dominated by two modes centred at about 1400 and 2000 nm d_{va} , indicating two sub-particle populations in this class. In the positive spectra of class 3, there is a nitrogen

15 containing organic compound marker at m/z 129 $C_5H_7NO^+$, which could originate from the OH oxidation of volatile organic compounds (VOCs) in the presence of NO_x on the seed particles, since the same peak was observed during simulation chamber studies with OH radicals reacting with α -pinene and/or toluene in the presence of NO_x . Besides, peaks at m/z 149 $C_4H_7O_2NO_3^+$ and 181 $C_4H_7O_4NO_3^+$ are associated with organonitrates that can form from the oxidation of VOCs in the presence of NO_x (Perring et al., 2013) and are expected to increase the light absorbing capability of the particles

20 (Canagaratna et al., 2007). In a related paper by Huang et al. (2018), we show that organonitrates favoured particle growth during the night at this location.

There is a 20.8% similarity of the total particle population to class 4 (“Secondary inorganic and amine like particles”). This class has the most prominent secondary inorganic signature and strongest correlation with the reference spectra for homogeneous mixtures of NH_4NO_3 and $(NH_4)_2SO_4$. In addition, it features marker peaks for amines at m/z 58 $C_2H_5NHCH_2^+$,

25 59 $(CH_3)_3N^+$, 86 $(C_2H_5)_2NCH_2^+$, 88 $(C_2H_5)_2NO/C_3H_6NO_2^+$, 118 $(C_2H_5)_2NCH_2^+$. Among all the representative mass spectra for seven particle classes, class 4 is relatively “clean” with the fewest peaks, indicating that the particles might be relatively fresh. The corresponding size range is between 500 to 1000 nm d_{va} .

A further 16.1% similarity of all particles was found to class 5 named “Potassium rich and aromatics coated dust like particles”. It has the most prominent peak at m/z 39 $K/C_3H_3^+$, aromatic marker peaks at 77 $C_5H_6^+$, 85 $C_7H_5^+$, 91 $C_7H_7^+$, 95

30 $C_7H_{11}^+$, 104 $C_8H_8^+$, 115 $C_9H_7^+$, and is correlated ($\gamma \geq 0.6$) with reference spectra of dust particles, especially agricultural soil dust. The ratio of m/z 39⁺/41⁺ is ~11.6, which is similar to the value for pure potassium containing inorganic samples measured by our LAAPTOF in the lab (13.5 ± 0.9). The contribution of organic fragments is likely the reason for the slightly lower value, as this ratio was determined to ~8 for humic acid and ~1.1 for α -pinene SOA (Shen et al., 2018). Hence, we assign the signal at m/z 39⁺ mainly to potassium. As suggested by previous studies, such potassium rich particles which

35 might originate from biomass burning, are often mixed with sulfate (Lin et al., 2017; Roth et al., 2016; Schmidt et al., 2017). This also holds true for this study, where for the class 5 particles exhibit characteristic peak at m/z 213 $K_3SO_4^+$. In addition, similar as class 3, class 5 also has two modes in its size distribution centred at about 500 and 800 nm d_{va} . Such sub-classes will be discussed in an upcoming paper.

There is a 5.7% similarity to class 6 with a size range of 400 to 1000 nm d_{va} named “Organosulfate coated dust like

40 particles”. It features organosulfate marker peaks at m/z 141 $C_2H_5OSO_4^-$, 155 $C_2H_3O_2SO_4^-$, and 215 $C_5H_{11}OSO_4^-$, which are consistent with signal from sulfate esters of glycolaldehyde/methylglyoxal, glyoxal/glycolic acid, and isoprene epoxydiols (IEPOX), respectively, observed by other SPMS in field measurements (Froyd et al., 2010; Hatch et al., 2011a, b). The ratio of m/z 39⁺/41⁺ is ~6.7 is closer to organics rather than to potassium. In addition, this class features a specific pattern of m/z



39⁺, 41⁺, and 43⁺ (which have much higher intensities than their interstitial peaks at m/z 40⁺ and 42⁺), and hydrocarbon and oxygenated organic fragments at m/z 53⁺, 55⁺, 63⁺, 65⁺, 67⁺, 69⁺, 71⁺, 73⁺, 81⁺, 83⁺, 85⁺, 95⁺, 97⁺, and 99⁺ likely from organic acids and biogenic SOA (Shen et al., 2018). Note that for the negative spectra we only find good correlations with reference spectra of sulfate and nitrate containing salts, as well as urban dust. Unfortunately, we don't have particular

5 reference spectra for organosulfate particles with corresponding anion markers.

Class 1 (5.0% similarity of all particles) is identified as "Calcium rich, metallic dust like particles". It contains calcium related signatures at m/z 40 Ca⁺, 56 CaO⁺, 57 CaOH⁺, 75 CaCl⁺, 96 Ca₂O⁺, and 112 (CaO)₂⁺, as well as some other metals including Na, Zn, Cu, Ba, and Pb. This class correlates well with all reference spectra of dust samples. Class 2 (4.3% similarity of all particles), "Aged soot like particles", is predominantly located in the small size range (200 to 600 nm d_{va}) and exhibits prominent elemental carbon (EC) patterns in both positive and negative mass spectra (characteristic C_n[±] progressions with up to $n = 12$). These mass spectra show a strong correlation to the reference spectra of soot particles, especially diesel soot ($\gamma = \sim 1$). Class 7 (4.6% similarity of all particles) is identified as "Mixed/aged particles", which contains no obvious characteristic features, and is correlated with most of the reference spectra. It has a relatively even and broad size distribution covering the whole size range that LAAPTOF is able to measure.

10

We observe intensive signal at m/z 138 Ba⁺ and 154 BaO⁺ in class 1, 5, 6 and 7, indicating a similar source of these particle types, which all have a good correlation with mineral and soil dust particles (Fig. 4). Prominent lead markers at m/z 206⁺ to 208⁺ can be found in each class, except class 4, which is further evidence for these particle to be relatively fresh. The marker peaks for lead appear broader because at higher m/z , we observe larger peak shifts that cannot be well corrected with the existing LAAPTOF software. Some peaks (e.g., m/z 78⁺ in class 3, m/z 98⁺ in class 4, and m/z 161⁺ in class 6) we were not able to identify. Note that even though we did not obtain spectra for pure ammonium sulfate or pure biogenic SOA particles in ambient air, it is still possible for such particles to be present. However, laboratory measurements show a very low sensitivity of the LAAPTOF to these types of particles, potentially due to their low absorbance at 193 nm. This low instrument sensitivity for these types of particles is very difficult to get to quantitative estimates about their abundance based on LAAPTOF measurements alone.

15

20

We emphasize here that the expression "rich" as used in this study only indicates a strong signal in the mass-spectra rather than a large fraction in mass, since there is no well-defined relationship between spectral signal and quantity. The sensitivities of the instrument to different species have yet to be established.

25

All the laboratory-based reference spectra used in this study are publicly available via the EUROCHAMP-2020 data base (www.eurochamp.org). Information on newly added reference spectra can be found in Table S2.

30 3.2 Quantification of single particle mass and the external mixing

We estimate the different single particle mass is based on the particle identification discussed above and on several assumptions on particle density and shape (cf. Sect. 2.2). And the fuzzy classification derived similarity (Fig. 3a) can be transferred into corrected number fractions (Fig. 3b) and further transferred into mass fractions (Fig. 3c) of seven externally mixed particle classes. Obvious changes can be observed when going from (a) to (b) to (c): compared with the similarity

35 fraction, the number fractions of class 3 and 4 decrease dramatically, while those of the other classes increase. This is because class 3 and 4 have higher fraction in the bigger size range (d_{va} : 600 to 2500 nm and d_p 400 to 1000 nm, respectively) which corresponds to the highest ODE values. And the other classes have bigger fraction in the smaller size range ($d_{va} < 500$ nm; $d_p < 300$ nm), which exhibits a relative lower ODE (cf. Fig. 1 and Fig. 2). Class 5 accounts for the second highest number fraction of the smaller particles and has a relatively high density. After correction, the number fraction of particles

40 attributed to this class has increased from 16.1% to 46.5% and become the dominating class with regards to particle number and mass. Class 3 is the second dominating class with respect to mass due to their bigger size, the cube of which is proportional to particle volume and mass. These observations demonstrate the crucial role of the corrections applied for



particle mass quantification for SPMS data. Note that we can obtain similar corrected number and mass fractions by using minimum, mean, and maximum ODE, respectively (Table S3). The observed external mixing of aerosol particles was temporally quite variable, e.g., class 6 “Organosulfate coated dust” dominated both particle number and mass at the beginning of the measurement until August 1st, while class 3 dominated the mass for August 5th to 10th, 21st to 24th, and 29th to 30th, and class 4 particles peaked twice on August 11th and 19th.

As discussed above, raw LAAPTOF data overestimate the particles with higher ODE, while the ones with lower ODE will be underestimated. After correction and further semi-quantification in mass, we can compare LAAPTOF result with the other quantitative instruments such as AMS. It turns out that the total mass of the quantified particles measured by LAAPTOF is ~12% (with maximum ODE), ~25% (mean ODE), and 104% (minimum ODE) of the total AMS mass with a collection efficiency of 0.5. In spite of this big uncertainty, LAAPTOF and AMS results have good correlations during some periods (P), such as P2, 4, and 5 (cf. Fig. 5 and Fig. S2), covering ~70% of the measurement time. Considering that AMS can only measure non-refractory compounds, the good correlation between AMS and LAAPTOF gives us a hint that the species measured by AMS might mainly originate from the particles of complex mixture of both refractory and non-refractory species. As shown in the upper panel of Fig. 5, the mass ratio of LAAPTOF to AMS has its lowest value in P3 and P5 when the AMS organic mass concentration is higher than in the other periods. This is in line with the fact that the LAAPTOF is less sensitive to pure organic species, such as oxalic, pinic, and cis-pinonic acids (Shen et al., 2018). However, the correlation coefficient values between LAAPTOF and AMS in P3 and P5 are quite different, indicating different dominating organic types, to which LAAPTOF might have different sensitivities. It is worth noting that during the whole campaign the sulfate mass fraction measured by AMS is largest in P3 (cf. Fig. S3). However, the LAAPTOF is not sensitive to some sulfate salts, e.g., pure ammonium sulfate (Shen et al., 2018), thus it is likely that such particles were dominating in P3.

3.3 Correlation of AMS and LAAPTOF results for non-refractory compounds

As shown in Fig. 6a, m/z 30 NO^+ measured by LAAPTOF has a good correlation ($\gamma = 0.6$) with ammonium measured by AMS, but LAAPTOF m/z 18 NH_4^+ doesn't ($\gamma = 0.3$, not shown in the figure), which was also found by Murphy et al. (2006). For nitrate (m/z 46 NO_2^- and m/z 62 NO_3^-), sulfate (panel c: sum of the marker peaks at m/z 32 S^- , 64 SO^- , 80 SO_3^- , 81 HSO_3^- , 96 SO_4^- , 97 HSO_4^- , 177 $\text{SO}_3\text{HSO}_4^-$, 195 $\text{H}_2\text{SO}_4\text{HSO}_4^-$), and organics (cations in panel d: at m/z 43 $\text{C}_3\text{H}_7/\text{C}_2\text{H}_5\text{O}/\text{CHNO}^+$, 58 $\text{C}_2\text{H}_5\text{NHCH}_2^+$, 59 $(\text{CH}_3)_3\text{N}^+$, 88 $(\text{C}_2\text{H}_5)_2\text{NO}/\text{C}_3\text{H}_6\text{NO}_2^+$, 95 $\text{C}_7\text{H}_{11}^+$, 104 C_8H_8^+ , 115 C_9H_7^+ , 129 $\text{C}_5\text{H}_7\text{NO}^+$, and anions in panel e: sum of the marker peaks at m/z 24 C_2^- , 25 C_2H^- , 26 $\text{C}_2\text{H}_2/\text{CN}^-$, 42 $\text{C}_2\text{H}_2\text{O}/\text{CNO}^-$, 45 COOH^- , 59 CH_2COOH^- , 71 $\text{CCH}_2\text{COOH}^-$, 73 $\text{C}_2\text{H}_4\text{COOH}^-$, 85 $\text{C}_3\text{H}_4\text{COO}^-$, 89 $(\text{CO})_2\text{OOH}^-$), there is a poor correlation ($\gamma \leq 0.4$) between these two instruments if we consider the entire measurement period. However, the fraction of LAAPTOF organic cations to the sum of ammonium and organic cations, $\text{org}/(\text{org}+\text{ammonium})$, anion fraction of $\text{org}/(\text{org}+\text{sulfate})$ and $\text{org}/(\text{org}+\text{nitrate})$, show better correlation between these two instruments (panel f to h), especially $\text{org}/(\text{org}+\text{nitrate})$. As shown in panel (g), a scatter plot of $\text{org}/(\text{org}+\text{nitrate})$ measured by LAAPTOF and AMS shows an exponential trend. A similar trend of carbonaceous/(carbonaceous+sulfate) were observed by another single particle mass spectrometer (PALMS) compared to AMS results for free tropospheric aerosol particles measured by Murphy et al. (2006).

Note that the aforementioned comparisons in this section are for the entire measurement period and demonstrate general correlations between these two instruments. Considering the different time periods, the correlations vary (cf. Fig. 6). All corresponding Pearson's correlation coefficient (γ) values for the comparisons of compounds measured by LAAPTOF and AMS are summarized in Table S4. During period 4, most of the γ values are above 0.6, suggesting good correlation, which is comparable with the mass comparison results discussed in Sect. 3.2.2. In particular, for the $\text{org}/(\text{org}+\text{nitrate})$ comparison, LAAPTOF and AMS show good/strong correlations for almost all the measurement time periods, the corresponding scatter plots are shown in Fig. S4. Period 2 and 4, covering > 50% measurement time, show similar exponential trends as the general fit in panel (g), while period 1, 3, and 5 show a linear correlation (especially in periods 3 and 5). This implies



different dominant particle types. Consistent with the observations: as shown in Fig. 3c, period 2 and 4 are dominated by class 3 particles and there are two class 4 burst events, while period 3 and 5 are dominated by class 5 particles containing more organics, which can also be validated by AMS results in Fig. 5 and Fig. S3. Therefore, we conclude that the relationship between LAAPTOF-org/(org+nitrate) and AMS-org/(org+nitrate) varies due to particle types.

- 5 Taken together, Fig. 6 and Fig. S4 might be useful to estimate the mass concentration of non-refractory compounds for LAAPTOF measurements without AMS in rural locations: ammonium mass concentrations can be estimated from panel (a), afterwards nitrate can be estimated from panel (f), then organics can be estimated by using panel (g) and/or Fig. S3 once the dominating particle types are determined, and finally the sulfate mass can be estimated from panel (h).

3.4 Particle sources of non-refractory components

- 10 The AMS can quantify the bulk particle mass of non-refractory species such as ammonium, nitrate, sulfate, and organics. LAAPTOF measurements suggest that ambient aerosol particles are often internal mixtures of ammonium, nitrate, sulfate, organics, and other characteristic species such as metals. In order to find out the dominant particle class/classes contributing to a certain non-refractory compound measured by AMS (namely compound donor class), we also need the class information of the single particles, which can be achieved by the single particle identification method described in Sect. 2.2, and assume
- 15 that LAAPTOF has a similar sensitivity to the same components of different particle classes. For nitrate measured by AMS, the dominating nitrate-donor particles with marker peaks at m/z 46 NO_2^- and 62 NO_3^- in LAAPTOF varied in different periods (Fig. 7): class 3 was the dominating class for the whole measurement campaign, but class 4 was dominant in its burst events (August 11th and 19th), while class 5 was dominant from August 25th to 29th. For ammonium measured by AMS, we have observed a similar trend as for class 4 particles, indicating that the ammonium AMS measured mainly originated from
- 20 this class. This can be reinforced by comparing with the time series of LAAPTOF marker peaks for ammonium and amine at m/z 18 NH_4^+ , 30 NO^+ , 58 $\text{C}_2\text{H}_5\text{NHCH}_2^+$, 59 $(\text{CH}_3)_3\text{N}^+$, and 88 $(\text{C}_2\text{H}_5)_2\text{NO}/\text{C}_3\text{H}_6\text{NO}_2^+$ (Fig. S5). For sulfate measured by AMS, we cannot infer the dominating donor class, since there is no comparable LAAPTOF class and fragments. This indicates again that this instrument is less sensitive or insensitive to some sulfate containing particles, such as pure ammonium sulfate. For organic compounds measured by AMS, it is also hard to find the comparable class and marker peaks
- 25 in LAAPTOF data, probably due to two reasons: one is the same as that for sulfate containing particles, and another one is that compared with AMS there are more fragments (cations and anions) arising from organics in LAAPTOF mass spectra. Nevertheless, we have found that peaks at m/z 129 $\text{C}_5\text{H}_7\text{NO}_3^+$ (arising from organonitrate) and 73 $\text{C}_2\text{H}_4\text{COO}^-$ (from organic acids) have a similar trend as the organics measured by AMS (cf. Fig. 8 b and c). At the beginning of the LAAPTOF measurements, the dominating organic donor class is class 6 (mainly contributing organic acids to be measured by AMS),
- 30 while at the end of the measurement period this changed to class 3 and 5 (mainly contributing organonitrate and organic acids, respectively). Apart from that, aromatic compounds mainly in class 5 could also contribute to the organic mass fraction measured by AMS, especially for the strongest organic burst event towards the end of the measurement period (cf. Fig. 8 d and e).

4 Conclusions and atmospheric implications

- 35 In this study, we used a combination of representative spectra obtained by fuzzy classification, laboratory based-reference spectra, marker peaks, and typical peak ratios for the improved single aerosol particle identification at a rural site in the upper Rhine valley near Karlsruhe city in Germany. Seven major particle classes were identified among a total of $\sim 3.7 \times 10^5$ single particles: class 1 is named “Calcium rich, metallic dust like particles”; class 2 “Aged soot like particles”; class 3 “Sodium salts like particles”; class 4 “Secondary inorganic and amine like particles”; class 5 “Potassium rich and aromatics
- 40 coated dust like particles”; class 6 “Organosulfate coated dust like particles”; and class 7 “Mixed/aged particles”. All



particles were internally mixed with organic and secondary inorganic compounds, i.e., ammonium, sulfate, and nitrate. According to our observation, these particles are expected to show a significant hygroscopicity due to their secondary inorganic contents (Fuzzi et al., 2015), as well as the presence of organosulfates (Thalman et al., 2017). The light absorption of soot particles might be enhanced by mixing with non-absorbing species such as most of the organic compounds that can reflect the light to the soot part (Bond et al., 2013). Organonitrates signatures found on class 3 particles are also expected to increase their light absorbing capability (Canagaratna et al., 2007) and assist nocturnal particle growth (the corresponding detailed discussion will be presented in a related paper by Huang et al. (2018) on the molecular composition of the organic aerosol particles. The good correlation of most of the particle classes and dust signatures suggests that condensation processes and heterogeneous chemistry have modified the dust particles during their transportation. For example, organosulfates coated dust could form from heterogeneous reactions of volatile organic compounds (VOCs), such as glyoxal, on mineral dust particles aged by reaction with e.g. SO₂ (Shen et al., 2016). Since organosulfates can form by heterogeneous reactions of IEPOX on acidic particles at low NO_x level (Froyd et al., 2010; Surratt et al., 2010), it is likely that they form also on acidified dust particles at the similar conditions. Our general observation of dominating aged and mixed aerosol particles is expected at a location about 2 hours downwind of nearest major emission sources (12 km distance to Karlsruhe at an average daytime wind speed of 1.7 m/s).

Based on the precise identification for particle classes and individual particles, we developed a semi-quantification method for single particles. As a result, class 3 changed from 43.5% (similarity) to 3.5% (corrected number fraction) corresponding to a mass fraction of 25.3%, becoming the second dominating class in mass; class 4 dramatically decreased from 20.8% to 2.4% corresponding to a mass fraction of 6.5%; becoming the least abundant class; class 5 changed from 16.1% to 46.5% corresponding to a mass fraction of 36%, becoming the dominating class in number and mass. The big difference between number-based and mass-based SPMS results has enforced the importance of particle mass quantification. Noteworthy, our semi-quantification approach requires several assumptions mainly regarding particle shape and density, which might cause ~540% uncertainties with the dominant ODE caused one. Regardless of such big uncertainty, we are the first to estimate single particle mass in SPMS studies. The resulting total particle mass show good correlations with total mass of non-refractory compounds, i.e., ammonium, nitrate, sulfate, and organic compounds measured by AMS in different periods, covering ~70% measurement time. This indicates these compounds might mainly be arising from the particles consisting of non-refractory and refractory components. Apart from the particle mass quantification, specific relationships of LAAPTOF ion intensity and AMS mass concentration results for non-refractory compounds have been found, especially for the fraction of org/(org+nitrate). The corresponding scatter plots might be useful to estimate the mass of these compounds in future LAAPTOF studies without quantitative instruments like AMS.

Considering a more precise correction and reduced quantification uncertainties, systematic measurements on different types of standard samples are still in need to help obtain more comprehensive sensitivity of this instrument. Multiple lines of evidence suggest that the LAAPTOF has a very low sensitivity for particles rich in such as pure ammonium sulfate and some organic species. In addition, particle size, density, morphology (shape), and chemical composition have impact on the ODE. Therefore, these factors need to be taken into account for a reasonable quantitative interpretation of SPMS data.

Employing particle class information for individual particles and specific marker peaks, this study is the first to assign non-refractory compounds measured by AMS to different classes of particles measured by SPMS. It turns out that nitrate measured by AMS was mainly from particle class 3. Ammonium measured by AMS was mainly arising from particle class 4. However, the dominating donor particle classes varied in different time periods during the measurements. Organic compounds measured by AMS were from organic acids (mainly on particle class 5 and 6), organonitrates (from class 3), and aromatic compounds (from class 5). During the entire measurement, dominating particle classes changed with respect to particle number and mass, and the donor classes for non-refractory compounds also varied substantially indicating changes of particles sources.



In spite of some uncertainties stemming from several assumptions and instrumental aspects, our study provides a good example for identifying particle class and individual particles. It opens a new way for quantitative interpretation of single particle data, and together with the complimentary results from bulk measurements by AMS we have shown how a better understanding of the internal and external mixing state of ambient aerosol particles can be achieved.

5 Data availability

LAAPTOF reference spectra are available upon request to the corresponding author and are available in electronic format via the EUROCHAMP DATA CENTER – Library of Analytical Resources of the EU project EUROCHAMP-2020 (<https://data.eurochamp.org/>, EUROCHAMP, 2018).

Author contributions

- 10 X.S. operated LAAPTOF and AMS during the whole field campaign, did the LAAPTOF data analysis, produced all figures, and wrote the manuscript. H.S. organized the campaign, provided suggestions for the data analysis, interpretation, and discussion. W.H. operated AMS during the whole campaign and did AMS data analysis. C.M. helped to operate the instruments, provided suggestions for the data analysis, interpretation, and discussion. R.R. helped to operate LAAPTOF. T.L. gave general advices and comments for this paper. All authors contributed to the final text.

15 Competing interests

The authors declare no conflict of interest.

Acknowledgements

- The authors gratefully thank the AIDA staff at KIT for helpful discussions and technical support, and the China Scholarship Council (CSC) for financial support of Xiaoli Shen and Wei Huang. Special thanks go to
- 20 Daniel Cziczko for discussions about particle identification and quantification methods, and to Nsikanabasi Umo for discussions about the coal fly ash sample.

References

- Ahern, A. T., Subramanian, R., Saliba, G., Lipsky, E. M., Donahue, N. M., and Sullivan, R. C.: Effect of secondary organic aerosol coating thickness on the real-time detection and characterization of biomass-burning soot by two particle mass spectrometers, *Atmos Meas Tech*, 9, 6117–6137, 2016.
- 25 Bahreini, R., Keywood, M. D., Ng, N. L., Varutbangkul, V., Gao, S., Flagan, R. C., Seinfeld, J. H., Worsnop, D. R., and Jimenez, J. L.: Measurements of secondary organic aerosol from oxidation of cycloalkenes, terpenes, and m-xylene using an Aerodyne aerosol mass spectrometer, *Environ Sci Technol*, 39, 5674–5688, 2005.
- Bond, T. C., Doherty, S. J., Fahey, D. W., Forster, P. M., Berntsen, T., DeAngelo, B. J., Flanner, M. G., Ghan, S., Karcher, B., Koch, D., Kinne, S., Kondo, Y., Quinn, P. K., Sarofim, M. C., Schultz, M. G., Schulz, M., Venkataraman, C., Zhang, H., Zhang, S., Bellouin, N., Guttikunda, S. K., Hopke, P. K., Jacobson, M. Z., Kaiser, J. W., Klimont, Z., Lohmann, U., Schwarz, J. P., Shindell, D., Storelvmo, T., Warren, S. G., and Zender, C. S.: Bounding the role of black carbon in the climate system: A scientific assessment, *J Geophys Res-Atmos*, 118, 5380–5552, 2013.



- Canagaratna, M. R., Jayne, J. T., Jimenez, J. L., Allan, J. D., Alfarra, M. R., Zhang, Q., Onasch, T. B., Drewnick, F., Coe, H., Middlebrook, A., Delia, A., Williams, L. R., Trimborn, A. M., Northway, M. J., DeCarlo, P. F., Kolb, C. E., Davidovits, P., and Worsnop, D. R.: Chemical and microphysical characterization of ambient aerosols with the aerodyne aerosol mass spectrometer, *Mass Spectrom Rev*, 26, 185–222, 2007.
- 5 DeCarlo, P. F., Kimmel, J. R., Trimborn, A., Northway, M. J., Jayne, J. T., Aiken, A. C., Gonin, M., Fuhrer, K., Horvath, T., Docherty, K. S., Worsnop, D. R., and Jimenez, J. L.: Field-deployable, high-resolution, time-of-flight aerosol mass spectrometer, *Anal Chem*, 78, 8281–8289, 2006.
- DeCarlo, P. F., Slowik, J. G., Worsnop, D. R., Davidovits, P., and Jimenez, J. L.: Particle morphology and density characterization by combined mobility and aerodynamic diameter measurements. Part 1: Theory, *Aerosol Sci Tech*, 38,
10 1185–1205, 2004.
- Froyd, K. D., Murphy, S. M., Murphy, D. M., de Gouw, J. A., Eddingsaas, N. C., and Wennberg, P. O.: Contribution of isoprene-derived organosulfates to free tropospheric aerosol mass, *P Natl Acad Sci USA*, 107, 21360–21365, 2010.
- Fuzzi, S., Baltensperger, U., Carslaw, K., Decesari, S., van Der Gon, H. D., Facchini, M. C., Fowler, D., Koren, I., Langford, B., Lohmann, U., Nemitz, E., Pandis, S., Riipinen, I., Rudich, Y., Schaap, M., Slowik, J. G., Spracklen, D. V., Vignati, E.,
15 Wild, M., Williams, M., and Gilardoni, S.: Particulate matter, air quality and climate: lessons learned and future needs, *Atmos Chem Phys*, 15, 8217–8299, 2015.
- Gallavardin, S., Lohmann, U., and Cizco, D.: Analysis and differentiation of mineral dust by single particle laser mass spectrometry, *Int J Mass Spectrom*, 274, 56–63, 2008.
- Gemayel, R., Hellebust, S., Temime-Roussel, B., Hayeck, N., Van Elteren, J. T., Wortham, H., and Gligorovski, S.: The
20 performance and the characterization of laser ablation aerosol particle time-of-flight mass spectrometry (LAAP-ToF-MS), *Atmos Meas Tech*, 9, 1947–1959, 2016.
- Gemayel, R., Temime-Roussel, B., Hayeck, N., Gandolfo, A., Hellebust, S., Gligorovski, S., and Wortham, H.: Development of an analytical methodology for obtaining quantitative mass concentrations from LAAP-ToF-MS measurements, *Talanta*, 174, 715–724, 2017.
- 25 Gross, D. S., Gälli, M. E., Silva, P. J., and Prather, K. A.: Relative sensitivity factors for alkali metal and ammonium cations in single particle aerosol time-of-flight mass spectra, *Anal Chem*, 72, 416–422, 2000.
- Hagemann, R., Corsmeier, U., Kottmeier, C., Rinke, R., Wieser, A., and Vogel, B.: Spatial variability of particle number concentrations and NO_x in the Karlsruhe (Germany) area obtained with the mobile laboratory 'AERO-TRAM', *Atmos Environ*, 94, 341–352, 2014.
- 30 Hatch, L. E., Creamean, J. M., Ault, A. P., Surratt, J. D., Chan, M. N., Seinfeld, J. H., Edgerton, E. S., Su, Y. X., and Prather, K. A.: Measurements of Isoprene-Derived Organosulfates in Ambient Aerosols by Aerosol Time-of-Flight Mass Spectrometry-Part 2: Temporal Variability and Formation Mechanisms, *Environ Sci Technol*, 45, 8648–8655, 2011a.
- Hatch, L. E., Creamean, J. M., Ault, A. P., Surratt, J. D., Chan, M. N., Seinfeld, J. H., Edgerton, E. S., Su, Y. X., and Prather, K. A.: Measurements of Isoprene-Derived Organosulfates in Ambient Aerosols by Aerosol Time-of-Flight Mass
35 Spectrometry - Part 1: Single Particle Atmospheric Observations in Atlanta, *Environ Sci Technol*, 45, 5105–5111, 2011b.
- Huang, W., Saathoff, H., Shen, X. L., Ramakrishna, R., Leisner, T., and Mohr, C.: Chemical characterization of highly functionalized organonitrates contributing to high night-time organic aerosol mass loadings and particle growth, *Environ Sci Technol*, to be submitted, 2018.
- Jeong, C. H., McGuire, M. L., Godri, K. J., Slowik, J. G., Rehbein, P. J. G., and Evans, G. J.: Quantification of aerosol
40 chemical composition using continuous single particle measurements, *Atmos Chem Phys*, 11, 7027–7044, 2011.
- Köllner, F., Schneider, J., Willis, M. D., Klimach, T., Helleis, F., Bozem, H., Kunkel, D., Hoor, P., Burkart, J., Leaitch, W. R., Aliabadi, A. A., Abbatt, J. P. D., Herber, A. B., and Borrmann, S.: Particulate trimethylamine in the summertime Canadian high Arctic lower troposphere, *Atmos Chem Phys*, 17, 13747–13766, 2017.



- Lin, Q. H., Zhang, G. H., Peng, L., Bi, X. H., Wang, X. M., Brechtel, F. J., Li, M., Chen, D. H., Peng, P. A., Sheng, G. Y., and Zhou, Z.: In situ chemical composition measurement of individual cloud residue particles at a mountain site, southern China, *Atmos Chem Phys*, 17, 8473–8488, 2017.
- Lu, D. W., Liu, Q., Yu, M., Yang, X. Z., Fu, Q., Zhang, X. S., Mu, Y. J., and Jiang, G. B.: Natural Silicon Isotopic Signatures Reveal the Sources of Airborne Fine Particulate Matter, *Environ Sci Technol*, 52, 1088–1095, 2018.
- 5 Marsden, N. A., Flynn, M. J., Allan, J. D., and Coe, H.: Online differentiation of mineral phase in aerosol particles by ion formation mechanism using a LAAP-TOF single-particle mass spectrometer, *Atmos Meas Tech*, 11, 195–213, 2018a.
- Marsden, N. A., Flynn, M. J., Taylor, J. W., Allan, J. D., and Coe, H.: Evaluating the influence of laser wavelength and detection stage geometry on optical detection efficiency in a single-particle mass spectrometer, *Atmos Meas Tech*, 9, 6051–6068, 2016.
- 10 Marsden, N. A., Ullrich, R., Möhler, O., Hammer, S. E., Kandler, K., Cui, Z., Williams, P. I., Flynn, M. J., Liu, D., Allan, J. D., and Coe, H.: Mineralogy and mixing state of North African mineral dust by on-line single-particle mass spectrometry, *Atmos Chem Phys Discuss*, <https://doi.org/10.5194/acp-2018-725>, 2018b.
- Middlebrook, A. M., Bahreini, R., Jimenez, J. L., and Canagaratna, M. R.: Evaluation of composition-dependent collection efficiencies for the aerodyne aerosol mass spectrometer using field data, *Aerosol Sci Tech*, 46, 258–271, 2012.
- 15 Murphy, D. M.: The design of single particle laser mass spectrometers, *Mass Spectrom Rev*, 26, 150–165, 2007.
- Murphy, D. M., Cziczo, D. J., Froyd, K. D., Hudson, P. K., Matthew, B. M., Middlebrook, A. M., Peltier, R. E., Sullivan, A., Thomson, D. S., and Weber, R. J.: Single-particle mass spectrometry of tropospheric aerosol particles, *J Geophys Res-Atmos*, 111, D23S32, doi: 10.1029/2006jd007340, 2006.
- 20 Noble, C. A. and Prather, K. A.: Real-time single particle mass spectrometry: a historical review of a quarter century of the chemical analysis of aerosols, *Mass Spectrom Rev*, 19, 248–274, 2000.
- Perring, A. E., Pusede, S. E., and Cohen, R. C.: An observational perspective on the atmospheric impacts of alkyl and multifunctional nitrates on ozone and secondary organic aerosol, *Chem Rev*, 113, 5848–5870, 2013.
- Pöschl, U.: Atmospheric aerosols: Composition, transformation, climate and health effects, *Angew Chem Int Edit*, 44, 7520–7540, 2005.
- 25 Pratt, K. A. and Prather, K. A.: Mass spectrometry of atmospheric aerosols-Recent developments and applications. Part II: On-line mass spectrometry techniques, *Mass Spectrom Rev*, 31, 17–48, 2012.
- Ramisetty, R., Abdelmonem, A., Shen, X. L., Saathoff, H., Leisner, T., and Mohr, C.: Exploring femtosecond laser ablation in single-particle aerosol mass spectrometry, *Atmos Meas Tech*, 11, 4345–4360, 2018.
- 30 Reinard, M. S. and Johnston, M. V.: Ion formation mechanism in laser desorption ionization of individual nanoparticles, *J Am Soc Mass Spectr*, 19, 389–399, 2008.
- Reitz, P., Zorn, S. R., Trimborn, S. H., and Trimborn, A. M.: A new, powerful technique to analyze single particle aerosol mass spectra using a combination of OPTICS and the fuzzy c-means algorithm, *J Aerosol Sci*, 98, 1–14, 2016.
- Roth, A., Schneider, J., Klimach, T., Mertes, S., van Pinxteren, D., Herrmann, H., and Borrmann, S.: Aerosol properties, source identification, and cloud processing in orographic clouds measured by single particle mass spectrometry on a central European mountain site during HCCT-2010, *Atmos Chem Phys*, 16, 505–524, 2016.
- 35 Schmidt, S., Schneider, J., Klimach, T., Mertes, S., Schenk, L. P., Curtius, J., and Borrmann, S.: Online single particle analysis of ice particle residuals from mountain-top mixed-phase clouds using laboratory derived particle type assignment, *Atmos Chem Phys*, 17, 575–594, 2017.
- 40 Shen, X. L., Ramisetty, R., Mohr, C., Huang, W., Leisner, T., and Saathoff, H.: Laser ablation aerosol particle time-of-flight mass spectrometer (LAAPTOF): performance, reference spectra and classification of atmospheric samples, *Atmos Meas Tech*, 11, 2325–2343, 2018.



- Shen, X. L., Wu, H. H., Zhao, Y., Huang, D., Huang, L. B., and Chen, Z. M.: Heterogeneous reactions of glyoxal on mineral particles: A new avenue for oligomers and organosulfate formation, *Atmos Environ*, 131, 133–140, 2016.
- Surratt, J. D., Chan, A. W. H., Eddingsaas, N. C., Chan, M. N., Loza, C. L., Kwan, A. J., Hersey, S. P., Flagan, R. C., Wennberg, P. O., and Seinfeld, J. H.: Reactive intermediates revealed in secondary organic aerosol formation from isoprene, *P Natl Acad Sci USA*, 107, 6640–6645, 2010.
- 5 Thalman, R., de Sa, S. S., Palm, B. B., Barbosa, H. M. J., Pohlker, M. L., Alexander, M. L., Brito, J., Carbone, S., Castillo, P., Day, D. A., Kuang, C. G., Manzi, A., Ng, N. L., Sedlacek, A. J., Souza, R., Springston, S., Watson, T., Pohlker, C., Pöschl, U., Andreae, M. O., Artaxo, P., Jimenez, J. L., Martin, S. T., and Wang, J.: CCN activity and organic hygroscopicity of aerosols downwind of an urban region in central Amazonia: seasonal and diel variations and impact of anthropogenic emissions, *Atmos Chem Phys*, 17, 11779–11801, 2017.
- 10 Wang, Z., King, S. M., Freney, E., Rosenoern, T., Smith, M. L., Chen, Q., Kuwata, M., Lewis, E. R., Pöschl, U., Wang, W., Buseck, P. R., and Martin, S. T.: The dynamic shapefactor of sodium chloride nanoparticles as regulated by drying rate, *Aerosol Sci Tech*, 44, 939–953, 2010.
- Weast, R. C.: *Handbook of chemistry and physics*, CRC Press Inc., Boca Raton Florida, 1987.
- 15 Williams, L. R., Gonzalez, L. A., Peck, J., Trimborn, D., McInnis, J., Farrar, M. R., Moore, K. D., Jayne, J. T., Robinson, W. A., Lewis, D. K., Onasch, T. B., Canagaratna, M. R., Trimborn, A., Timko, M. T., Magoon, G., Deng, R., Tang, D., Blanco, E. D. L. R., Prévôt, A. S. H., Smith, K. A., and Worsnop, D. R.: Characterization of an aerodynamic lens for transmitting particles greater than 1 micrometer in diameter into the Aerodyne aerosol mass spectrometer, *Atmos Meas Tech*, 6, 3271–3280, 2013.
- 20 Wonaschuetz, A., Kallinger, P., Szymanski, W., and Hitzenberger, R.: Chemical composition of radiolytically formed particles using single-particle mass spectrometry, *J Aerosol Sci*, 113, 242–249, 2017.
- Zawadowicz, M. A., Froyd, K. D., Murphy, D., and Cziczo, D. J.: Improved identification of primary biological aerosol particles using single particle mass spectrometry, *Atmos Chem Phys*, 17, 7193–7212, 2017.
- Zhou, Y., Huang, X. H. H., Griffith, S. M., Li, M., Li, L., Zhou, Z., Wu, C., Meng, J. W., Chan, C. K., Louie, P. K. K., and Yu, J. Z.: A field measurement based scaling approach for quantification of major ions, organic carbon, and elemental carbon using a single particle aerosol mass spectrometer, *Atmos Environ*, 143, 300–312, 2016.
- 25



Table 1: Particle fuzzy class number, symbol colour, and names. “rich” used in the names stands for the strong spectral signal rather than the real mass fraction. Class 7 is named “mixed/aged particles” because particles in this class have almost all the marker peaks from the other classes.

Class no.	Symbol colour	Name
1	red	Calcium rich, metallic dust like particles
2	black	Aged soot like particles
3	blue	Sodium salts like particles
4	orange	Secondary inorganic and amine like particles
5	green	Potassium rich and aromatics coated dust like particles
6	purple	Organosulfate coated dust like particles
7	grey	Mixed/aged particles

5

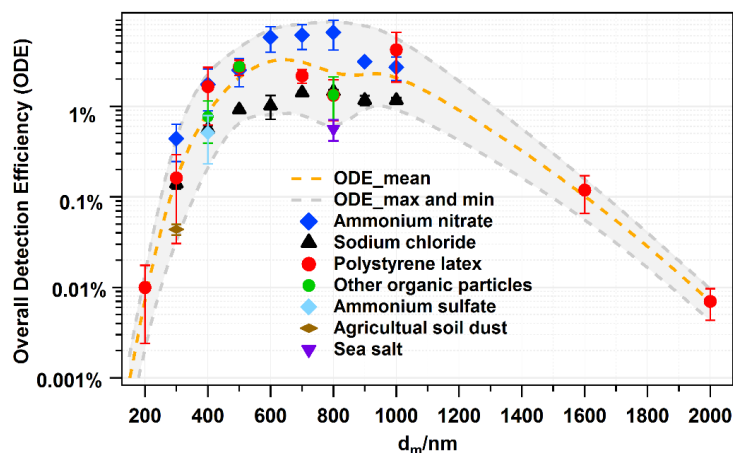


Figure 1: Overall detection efficiency (ODE) of LAAPTOF for different types of particles as a function of the mobility diameter (d_m), adapted from Shen et al. (2018). Dashed lines are fitting curves for maximum, mean and minimum values of ODE. For other organic particles (green), ODE at 400 nm is the data from secondary organic aerosol (SOA) particles from α -pinene ozonolysis, ODE at 500 nm is the data from humic acid, and ODE at 800 nm is data from humic acid ($1.9 \pm 0.3\%$), oxalic acid ($0.3 \pm 0.1\%$), pinic acid ($1.6 \pm 0.1\%$), and cis-pinonic acid ($1.9 \pm 0.7\%$). SOA particles were formed in the Aerosol Preparation and Characterization (APC) chamber and then transferred into the AIDA chamber. Agricultural soil dust (brown) were dispersed by a rotating brush generator and injected via cyclones into the AIDA chamber. Sea salt particles (purple) were also sampled from AIDA chamber. The other aerosol particles shown in this figure were generated from a nebulizer and size-selected by a DMA. Note that there is uncertainty with respect to particle size due to the particle generation method. The nebulized and DMA sized samples have relative smaller standard deviation (SD) from Gaussian fitting to the measured particle sizes. PSL size has the smallest size SD (averaged value is 20 nm) and the corresponding relative SD (RSD = SD divided by the corresponding size) is ~6%, since the original samples are with certain sizes. The other nebulized samples have standard deviations ranging from 70 to 120 nm SD and 3 to 23% RSD. Particles sampled from AIDA chamber have much bigger size SD: ~70 nm for SOA (17% RSD), ~200 nm for agricultural soil dust (~60% RSD), and sea salt particles (~34% RSD). Considering this uncertainty, we have chosen size segment of 100 nm (± 50 nm) for correction, e.g., particles with size of 450 to 550 nm will use the ODE at 500 nm particle number correction.

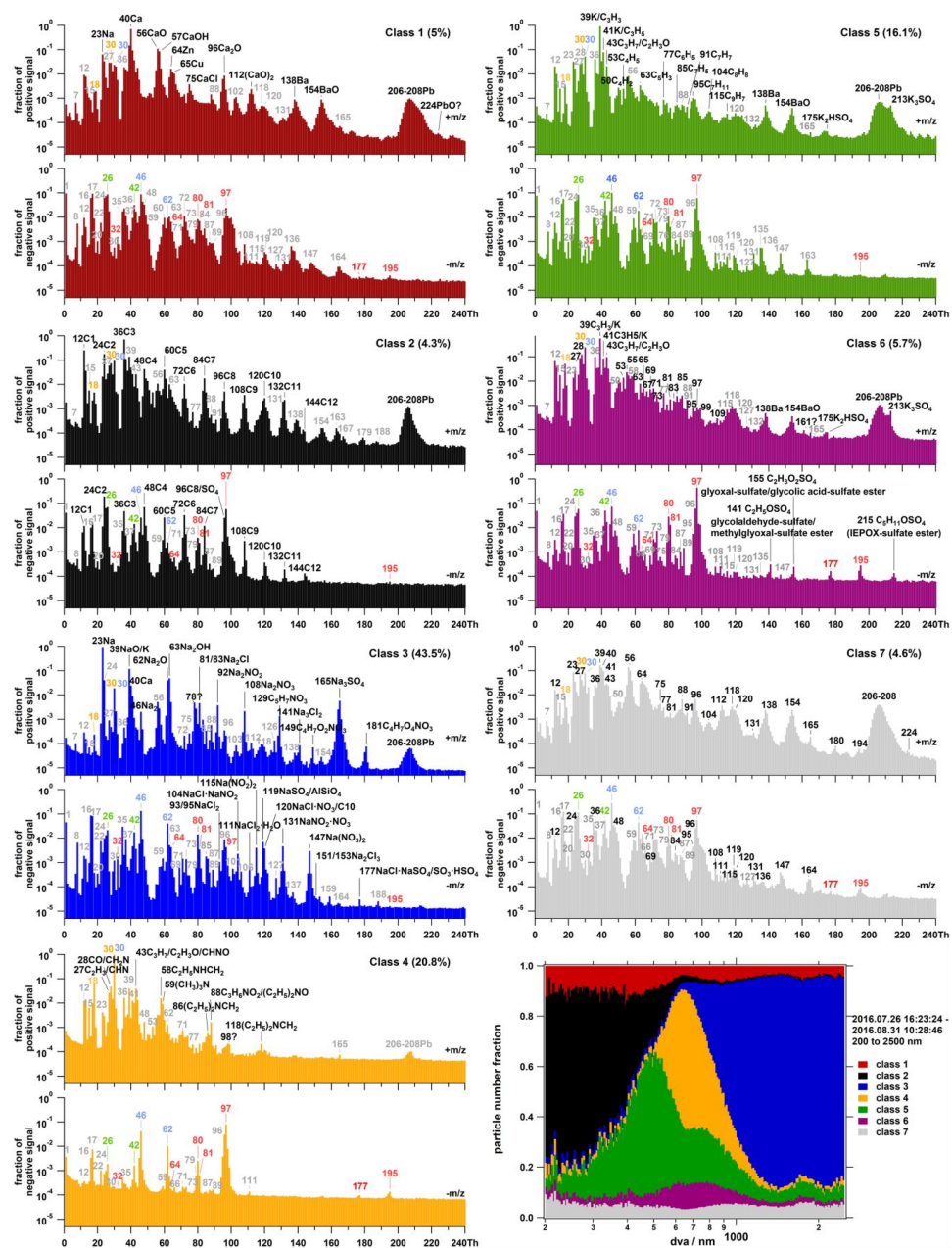


Figure 2: Representative mass spectra and size resolved number fraction for seven particle classes measured during the field campaign TRAM01, based on fuzzy classification according to fuzzy *c*-means clustering algorithm. The percentage in each pair of spectra gives us information about the similarity of the total aerosol particles to different classes. The red, blue, and orange labels represent the signatures for sulfate (32 S⁻, 64 SO₂⁻, 80 SO₃⁻, 81 HSO₃⁻, 97 HSO₄⁻, 177 SO₃HSO₄⁻, and 195 HSO₄H₂SO₄⁻), nitrate (30 NO⁻, 46 NO₂⁻, and 62 NO₃⁻) and ammonium (18 NH₄⁺ and 30 NO⁺). The green labels represent the organic compounds (26 C₂H₂/C⁻ and 42 C₂H₂O/CNO⁻). Grey labels represent the background fragments that exist for every particle class, while the black ones are the signatures for different classes.

5

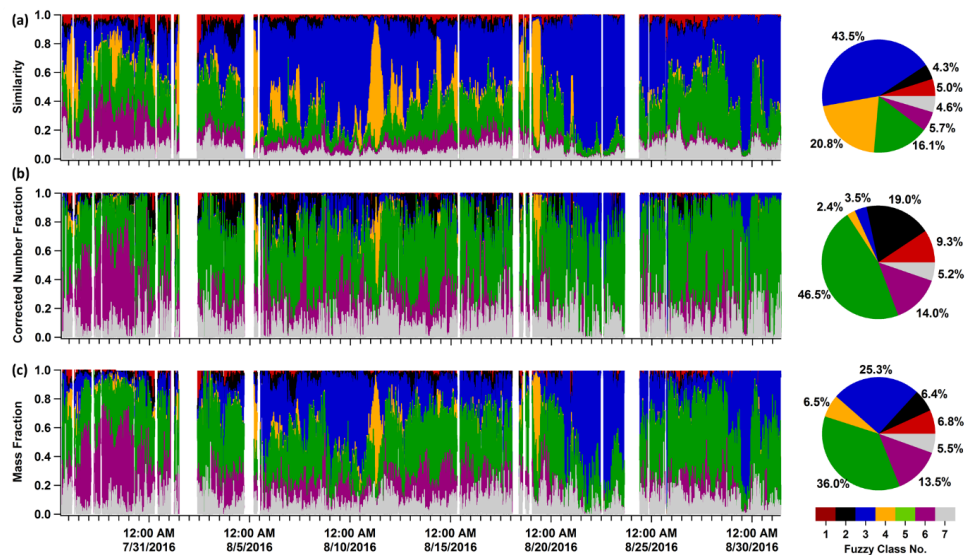


Figure 3: Time series of the similarity, corrected number fraction, and mass fraction of seven major particle classes and the corresponding pie charts for total fractions. The timeline covers the whole LAAPTOF measurement in this campaign. Note that, the correction here is based on ODE mean value.

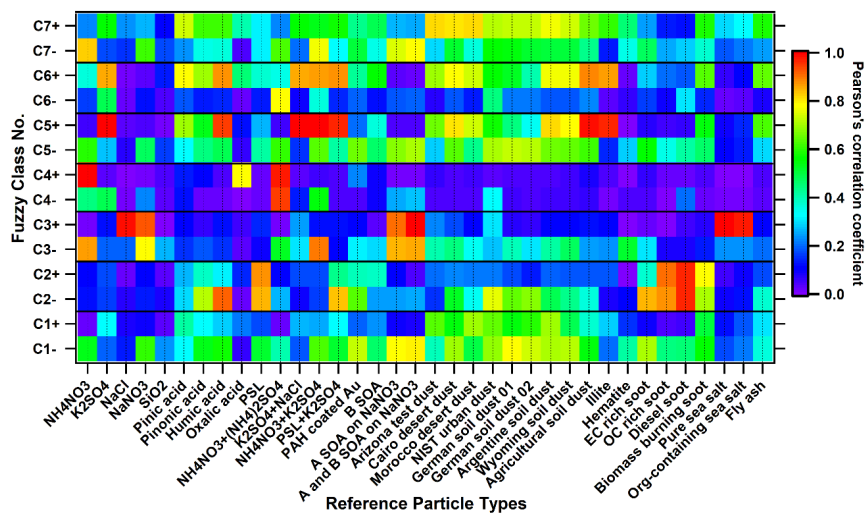


Figure 4: Correlation diagram of fuzzy classification results (7 classes, C1 to C7) and 36 laboratory-based reference spectra. Correlation results for the positive and negative spectra (e.g., for C1) are in the separated rows (e.g., C1+ and C1-). PAH is short for poly(allylamine hydrochloride), B SOA is short for biogenic SOA (α -pinene SOA in this study), A SOA is short for anthropogenic SOA (toluene SOA in this study), biomass burning soot is the lignocellulosic char from Chestnut wood. Note that, the strong and good correlations mentioned in the paper stand for Pearson's correlation coefficient $\gamma \geq 0.8$ and $\gamma \geq 0.6$, respectively.

5

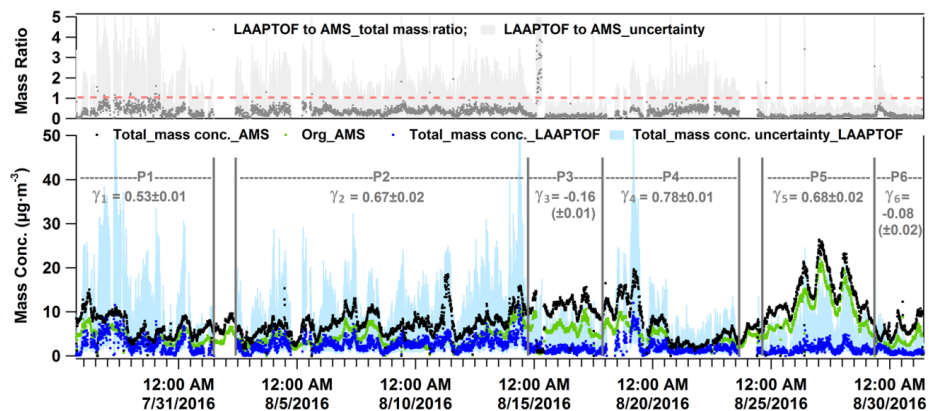


Figure 5: Time series of total mass ratio of LAAPTOF to AMS, LAAPTOF total mass, AMS total mass and organic mass concentration measured by AMS. γ is a Pearson's correlation coefficient. P1 is Period 1 from 7/26/2016 16:23 to 8/1/2016 11:43; P2 from 8/2/2016 09:43 to 8/14/2016 17:53; P3 from 8/14/2016; P4 from 8/17/2016 21:13:00 to 8/23/2016 15:33; P5 from 8/24/2016 15:03 to 8/29/2016 08:33; P6 from 8/29/2016 08:43 to 8/31/2016 09:13. Zoom in figures for P1, 2, 4, and 5 can be found in Fig. S2, as well as the corresponding scatter plots for LAAPTOF and AMS data comparison.

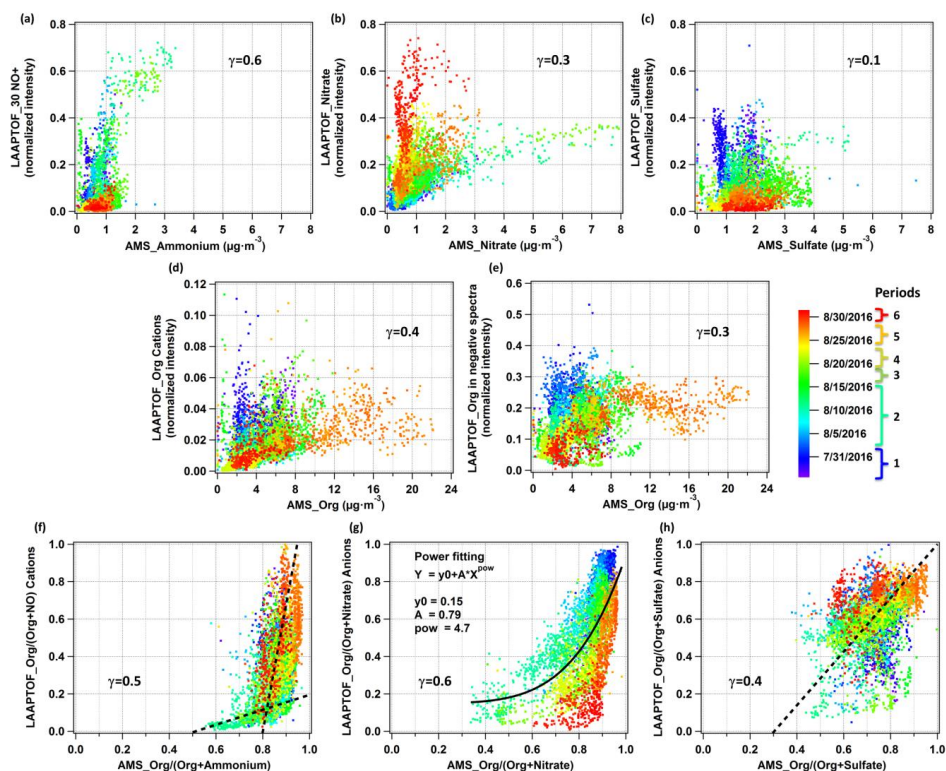


Figure 6: Comparison of non-refractory compounds measured by LAAPTOF and AMS: The normalized intensity of (a) 30 NO^+ ; (b) nitrate ($46 \text{ NO}_2^- + 62 \text{ NO}_3^-$); (c) sulfate ($32 \text{ S}^- + 64 \text{ SO}^- + 80 \text{ SO}_3^- + 81 \text{HSO}_3^- + 96 \text{ SO}_4^- + 97 \text{ HSO}_4^- + 177 \text{ SO}_3\text{HSO}_4^- + 195 \text{ H}_2\text{SO}_4\text{HSO}_4^-$); (d) sum of positive organic markers at m/z 43 $\text{C}_3\text{H}_7/\text{C}_2\text{H}_3\text{O}/\text{CHNO}^+$, 58 $\text{C}_2\text{H}_2\text{NHCH}_2^+$, 59 $(\text{CH}_3)_3\text{N}^+$, 88 $(\text{C}_2\text{H}_5)_2\text{NO}/\text{C}_3\text{H}_6\text{NO}_2^+$, 95 $\text{C}_7\text{H}_{11}^+$, 104 C_8H_8^+ , 115 C_9H_7^+ , and 129 $\text{C}_5\text{H}_7\text{NO}^+$ and (e) sum of the negative organic markers at m/z 24 C_2^- , 25 C_2H^- , 26 $\text{C}_2\text{H}_2/\text{CN}^-$, 42 $\text{C}_2\text{H}_2\text{O}/\text{CNO}^-$, 45 COOH^- , 59 CH_2COOH^- , 71 $\text{CCH}_2\text{COOH}^-$, 73 $\text{C}_2\text{H}_4\text{COOH}^-$, 85 $\text{C}_3\text{H}_4\text{COOH}^-$, and 89 $(\text{CO})_2\text{OOH}^-$ measured by LAAPTOF are plotted versus the mass concentration of ammonium, nitrate, sulfate, and organics measured by AMS, respectively. Comparison of LAAPTOF organic cations and NO^+ fractions ($\text{Org}/(\text{Org}+\text{NO})$), organic anions and sulfate fractions, as well as organic anions and nitrate fractions to the AMS mass fractions are also plotted in (f), (g), (h), respectively. Each point is 10 min averaged data, and there are 4483 points in each scatter plot. Dashed line in panel (f) and (h) are used to guide the eyes, while the curve in panel (g) is from the fitting result. Colour scale is related to the timeline, including periods 1 to 6.

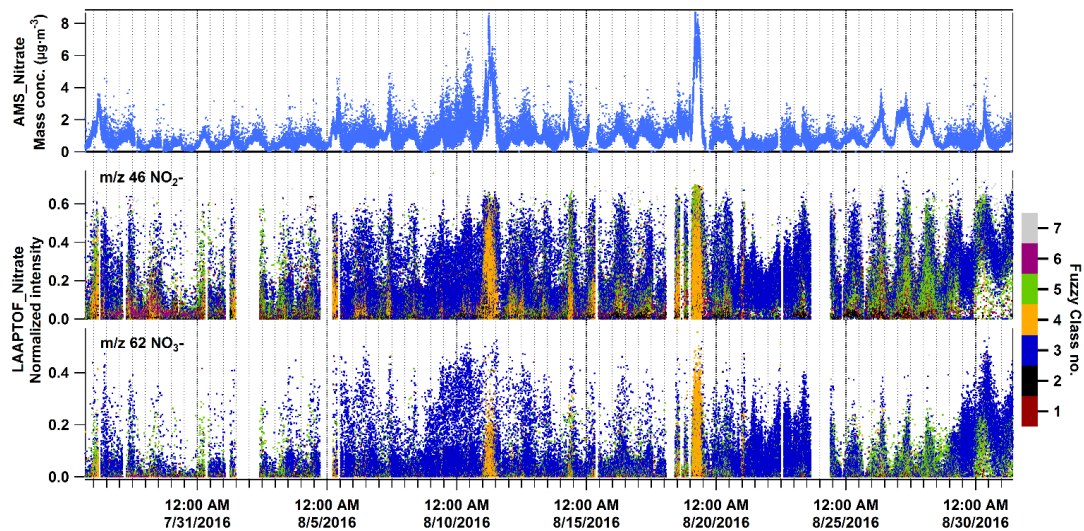


Figure 7: Time series of nitrates measured by AMS in mass concentration and LAAPTOF in ion intensity, respectively. Normalized intensity refers to the fragment intensity divided by sum of all the ion intensities. Marker peaks for nitrates are at m/z 46 NO_2^- and 62 NO_3^- in LAAPTOF spectra, thus we use them to represent nitrates.

5

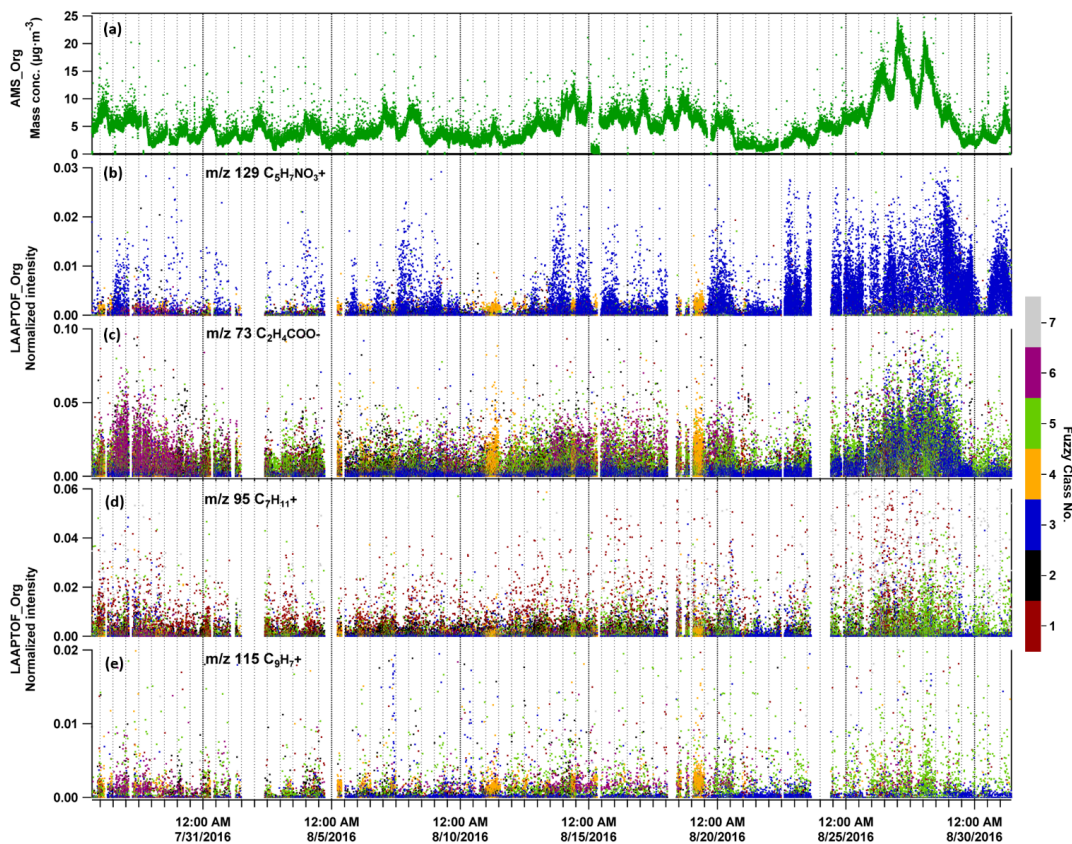


Figure 8: Time series of organic species measured by AMS in mass concentration and LAAPTOF in ion intensity, respectively. Normalized intensity refers to the fragment intensity divided by sum of all the ion intensities. In LAAPTOF spectra, peaks at m/z 129 $C_3H_7NO_3^+$ is arising from organonitrate, 73 $C_2H_4COO^-$ from organic acids, and 95 $C_7H_{11}^+$ and 115 $C_9H_7^+$ are from aromatic compounds.

5